2015

Conformational changes of von Willebrand Factor multimer subject to extensional flows

XINTONG RONG
Lehigh University

Conformational Changes of von Willebrand Factor Multimer Subject to Extensional Flows

by

Xintong (Ethan) Rong

A Thesis

Presented to the Graduate and Research Committee

of Lehigh University

in Candidacy for the Degree of

Master of Science

in

Mechanical Engineering

Lehigh University

Aug 2015

This thesis is accepted and approved in partial fulfillment of the requirements for the Master of Science.

_____

Date

_____

Thesis Advisor: Professor Alparslan Oztekin

_____

Department Chair: Professor Gary Harlow

Acknowledgements

Through the one year-effort, this thesis, which is focus on conformational changes of von Willebrand Factor multimer subject to extensional flows, has already been completed. Many people in my life, including my family, mentor, and friends, indeed made a profound contribution to my work, without which I will never reach such an achievement. Therefore, it is necessary to appreciate some of the most important people who have offered me much precious help and support during this tough period.

First and foremost, my mentor, Prof. Alparslan Oztekin, who ever gave me masterful guidance academically during my research period deserves the most appreciation. He is one of the most excellent professors I have ever met who care me so much in my everyday life. Also, it is his excellence, creation, energy, patience and devotion to research that strongly influenced me. Under his guidance, I really realize my interest in this field, and it is also his encouragement that helped me reach such an achievement.

In addition, my parents and friends also deserve my sincere appreciation for helping me in many aspects. It is impossible for me to achieve my goal without their academic, emotional and financial help. Through this unforgettable experience, I do realized that I must always keep passion and creation while doing anything meaningful, so as to reach an achievement. Thus, I regard this thesis as a gift for their incredible patience, support and love.

Contents

List of Figures and Tables

Abstract

The von Willebrand Factor (vWF) is a large multimeric protein in the blood that aids in blood clotting. It activates the clotting cascade at specific time and specific place, which is one of the human body's masterpieces in targeted molecular manipulation. Hydrodynamic forces trigger conformational changes of vWF, by which its potency and reactivity are regulated. In this thesis, inspiration is taken from novel findings in vWF experiments. The present study aims to describe the behaviors in this process within the context of polymer science. Understanding the basic physical principle helps us to develop targeted drug therapy, which is capable to deliver drug wherever and whenever needed.

After the introduction of blood clotting process, researchers in our group propose a novel bead-spring model. Contrary to classic bead-spring model that each bead is connected by one type of spring, the new model's beads are connected by finitely extensible nonlinear elastic (FENE) springs and Hookean springs consecutively. The motivation is that the A2 domain, which will undergo significant unfolding process during stretching experiments, has been proven to be very flexible. Instead of modeling a monomer as one bead, more details inside each monomer and more complexity of vWF multimer have been captured by modeling vWF monomers as a highly flexible A2 domain with relatively very rigid domains on either side of A2. The A2 domain is modeled as a finitely extensible nonlinear elastic (FENE) spring, which is capable of significant extension. At each end of the spring is a spherical bead, which is used to represent neighboring rigid domains. In addition, the adjacent monomers are connected by a tight harmonic spring successively to form the vWF

multimers of desired length.

In an effort to validate our mythology and generalize our results quantitatively, it is necessary to study the vWF multimers represented by this noval model in both relaxation without flow scenarios and unfolding in response to specific flow circumstances.

Since other researchers in our group have already studied the behaviors of a single vWF multimer unfolding in response to shear flow, here we extend our research further to the behaviors in response to extensional flow. The first and second chapter of this thesis state a brief introduction of blood clotting process and the simulation methodology which uses the noval model proposed by researchers in our group. The third chapter includes all the relevant calculation, analysis, results and discussion in details. Finally, the last chapter presents a comprehensive summary of the behaviors of vWF unfolding process in respond to extensional flow. From the research, it concludes that flow intensity and molecular size do have profound influences on the behavior characteristics of vWF multimer unfolding process. A certain length chain has been proven to unfold much faster in response to stronger extensional flow. Moreover, longer vWF chains have been proven to have more potential to unfold. Thus, comparing with shear flow, vWF multimers will unfold faster and stronger in response to extensional flow.

Chapter 1 Introduction

1.1 Biopolymer manipulation inspired by blood clotting

In the past few decades, one of the major motivations in the study of polymer science has become the desire to utilize the power to control the behavior of biopolymers. [1] The thermodynamics, kinetics, and polymer chain structure knowledge in the field of polymer science could work together to strengthen a techniques for the manipulation, which could also possibly make many significant breakthroughs in polymer science. [2] The biopolymer manipulation, "protein unfolding", which used molecule manipulation techniques, deserves consideration. One of the protein unfolding technique is implemented in an indirect way – through the presence of fluid flows.

Hemostasis is a well-balanced process that can prevent excessive blood loss after vascular injury involving a complex interplay between a plethora of agonists and antagonists. [3] Under special conditions, platelet-rich thrombi will occlude the vascular lumen, often resulting in cardiovascular disease, which is still the leading cause of death in the modern world. [3] The function of von Willebrand Factor (vWF) is related to the unfolding of it in response to the presence of various fluid flows. vWF is also able to bind to both subendothelial structures in the injured vessel wall and circulating blood platelets by supporting the formation of a platelet-rich plug that will prevent bleeding and promote wound healing. [4,5] In this thesis, since studying the characteristic of vWF protein under shear flow has already been accomplished, extending the topic further to the extensional flow is the primary focus. Moreover, the results gained from this study will suggest approaches to achieve a specific medical help in human body, such as targeted drug therapy.

1.2 Blood Clotting Process – Coagulation

The blood clotting process, which is also named coagulation, is one of the most complicated phenomena in human body. [4] The mechanism of coagulation includes activation, adhesion, and aggregation of platelets and more. Once the injury appears, vWF will not interact circulating platelets. [6] Under this situation, endothelial cells no longer form a barrier wall between the inside blood and the extracellular matrix. Collagens, constituting almost of the extracellular matrix, interact with vWF and then result in the deposition of vWF on the damaged vessel wall in response to fluid flows. It is possible for vWF to bind platelets with affinity areas sufficiently to snare them from rapidly flowing blood and retains them at the injury place. However, platelets have no measurable interaction with vWF in the circulation, but adhere prompt to exposed immobilized vWF. [7] This localization of platelets to the extracellular matrix promotes collagen interaction with platelet glycoprotein VI. Binding of collagen to glycoprotein VI leads a signaling cascade that results in activation of platelet integrin, which indirectly tight binding of platelets to extracellular matrix. Activated platelets release the contents of stored granules into the blood plasma, which in turn, activate additional platelets.

1.3 Structure and Functionality of Von Willebrand Factor

von Willebrand Factor is one of the main actuators in the blood clotting process. Once secreted into the plasma, circulating vWF will keep its ultra-large state and are the most active ones by the time they provide multiple interactive sites for binding. [3] The ultra-large vWF multimer becomes smaller fragments by a disintegrin and metalloprotease named ADAMTS13 and undergoes scission to shorten the chain to its typical length. [8–

12] After cleavage, the vWF concatemers in plasma are able to contain 40 to 200 monomers that can be stretched by hydrodynamics forces. In addition, multimeric vWF has many binding sites for platelets and collagen, and experiences highly significant hydrodynamic forces in the circulating system. It has been studied that vWF has force-sensing capability: the protein adopts a compact shape in normal circulatory state where extensional rates range from hundreds to a few thousand per second; for extensional rates greater than 5000 s^{-1}. As vWF changes conformation to an elongated shape, it increases its interaction with platelets and collagen. (Fig. 1.3 (B))

Model proposed by Ouyang [30] suggests that each pro-vWF subunit consists of four types of repeated domains that are arranged in the sequence D1-D2-D'-D3-A1-A2-A3-D4-B1-B2-B3-C1-C2-CK (Fig. 1.3.(A)). Each domain contains the various chemical functionalities required for the interactions between vWF and its surroundings. [5] Among all domains in vWF, A2 domain is a force-sensitive domain that lacks a long-range disulfide and thus will unfold by hydrodynamic forces in extensional flows. [5,12] Unfolding of A2 has an important functionality that dictates the cleavage of vWF multimers through with ADAMTS-13.

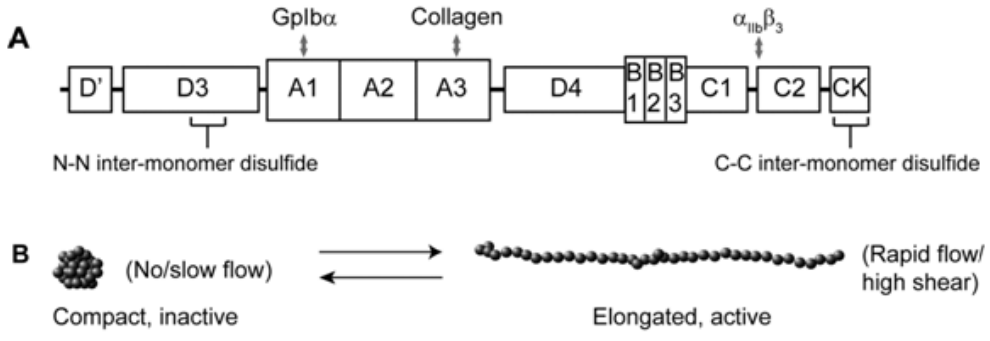

Fig. 1.3 (A) Schematic illustration of vWF's domains. (B) Possible mechanism of flow-induced conformational change.

This is a normal process that will occur in the bloodstream, which is a way to limit the length of vWF. [7,12,30] A1 domain strongly interacts with platelets on their surfaces. Remarkably, since A1 domain is the most positively charged domain in vWF and the face of GP1ba receptor is negatively charged, electrostatic interactions aid in coupling of this ligand-receptor pair. [5,7] The role of this interaction appears to be the incorporation of platelets into plug, which initiate the blood-clotting cascade. Also, A1 domain has binding sites for collagens, although mutagenesis studies suggest the major collagen binding site of multimeric vWF is within domain A3. A1 binds collagen VI, a microfibrillar collagen and binds collagens I and III as well. The fluid flow activation is required for vWF multimer to function. For example, strong extensional flow or shear flow, which is normal to damaged vessel wall, is able to elongate vWF multimer that will expose multiple binding sites in a physiological environment and facilitate blood clotting process at last. This unique characteristic of vWF multimer is certainly inspiring. Comprehensive studies will help to develop novel drug delivery method that use a molecule to carry specific drug directly to the target sites as a vehicle and therefore diminish the side effects. Study on manipulating these characteristics of vWF multimer is very necessary to design targeted drugs. Therefore, based on the research achievements by Ouyang [30], which is mainly focused on the presence of shear flow in blooding clotting model, it is requisite to further extend this topic to the presence of extensional flow to consummate this topic.

Chapter 2 vWF Simulation Methodology

2.1 von Willebrand Factor Model

Previous researcher in our group has already successfully developed a new model which attempts to more realistically describe molecular architecture inherent in the protein will be presented. This model can capture the aspect which we believe to be a primary mechanical response of a single monomer. It is accomplished by modeling vWF monomers as an extensible domain with relatively rigid domains on either side of it. The A2 domain has been shown to undergo significant unfolding process in rapid flow conditions. At each end of the spring is a spherical bead which represents neighboring rigid domains (Fig. 2.1). Adjacent monomers are connected by a relatively stiff harmonic spring between beads of each monomer, so as to form the vWF multimers of desired length. This innovative improvement of the previous typical coarse-grain vWF models introduces a simple model, which, however, is capable of capturing the structural complexity of vWF multimers.

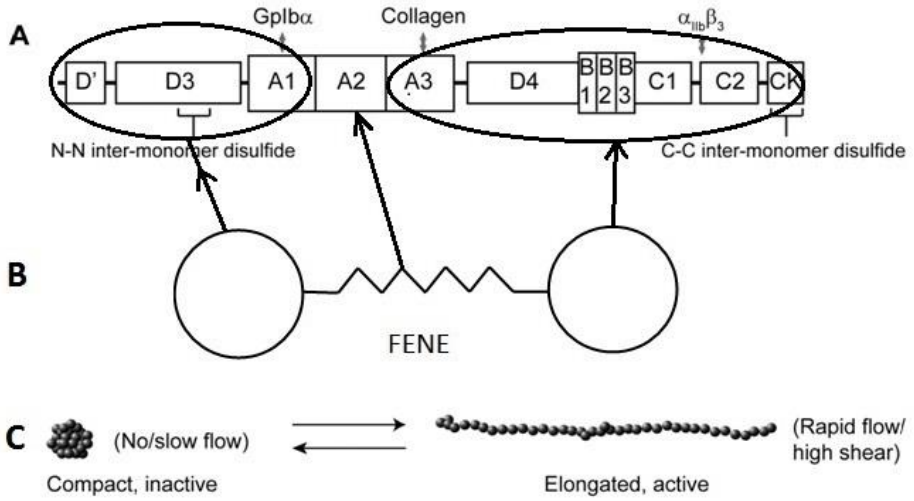

Fig. 2.1 (A) Schematic illustration of vWF's domains. (B) The vWF monomer model containing two rigid beads connected by a highly flexible FENE spring. (C) Possible mechanism of flow-induced conformational change.

2.2 Numerical Method

The vWF model in this thesis is developed from the bead-spring model which has already been used by many investigators. [15,16] In the present model, each monomer owns one FENE spring that connects its two beads. Experimental evidence demonstrates that the A2 domain of each monomer will undergo unfolding process due to hydrodynamic forces applied on vWF molecules under rapid blood flow conditions. From a mechanical response point of view, it is more realistic to represent the extensible part of each monomer as a FENE spring than to represent the whole monomer as a single bead. Moreover, the use of FENE spring can be computed more efficiently than modeling the A2 domain as a relatively long series of beads. As for the pair potential between beads, a Lennard-Jones pairwise interaction will be applied.

2.2.1 Brownian dynamics

The Brownian dynamics (BD) is a simplified version of Langevin dynamics (LD), in which the average acceleration will be neglected, so that BD is also called non-inertial dynamics. The BD simulation, an efficient method for studying molecular dynamics, is proposed as early as 1978 by D.L. Ermak and J.A. McCammon. [17] They used BD simulations of short chains with hydrodynamic interaction (HI) at equilibrium. Meanwhile, Fixman developed the mathematical background for BD simulations of polymer chains in hydrodynamic flow conditions.

2.2.2 Physical forces

The drag force is a type of hydrodynamic force which flowing solvent exerts on the polymer and is given by

$$\boldsymbol{F}_i^D = -\zeta(\dot{\mathbf{r}}_i - \boldsymbol{v}_i) = -\zeta(\dot{\mathbf{r}}_i - (\nabla \boldsymbol{u})^T \mathbf{r}_i) \quad (1)$$

where ζ is the drag coefficient, $\dot{\mathbf{r}}_i$ is the velocity of the bead i, $\boldsymbol{v}_i$ is the undisturbed velocity field and $\nabla \boldsymbol{u}$ is the velocity gradient tensor. Similar to Hoda and Larson's work [13], variables are made dimensionless by scaling length with $\sqrt{k_b T/H}$, force with $\sqrt{H k_b T}$, and time with ζ/H. Here k_b is the Boltzmann constant, T is the absolute temperature and H is the spring constant in the FENE spring term. $\boldsymbol{F^S}$ is either a FENE spring force or a harmonic spring force, which account for the connectivity of the chain. Dimensionless FENE springs are described as

$$\boldsymbol{F}_{i,FENE}^S = \frac{\boldsymbol{Q}_i}{1 - {Q_i}^2/Q_0^2} \quad (2)$$

where $\boldsymbol{Q}_i = \mathbf{r}_{i+1} - \mathbf{r}_i$ and Q_i is the magnitude of $\boldsymbol{Q}_i$. Q_0 is the maximum extended length for the FENE spring. The expression for the harmonic springs is given by

$$\boldsymbol{F}_{i,Harmonic}^S = k \frac{\boldsymbol{Q}_i}{Q_i}(Q_i - \dot{Q}) \quad (3)$$

The harmonic force of strength k keeps the average distance between connected monomers stiffly constrained to relatively small fluctuations around $\dot{Q}$. To ensure this, the value of k is chosen to be 100. $\dot{Q}$ = 4 (21.54nm) which is larger than two times of the bead radius, determined from size considerations for vWF monomers.

The self-association between different monomers, which collapses the vWF multimer into a relatively compact globule, is represented by a pairwise truncated Lennard-Jones

interaction force that acts between beads.

$$\boldsymbol{F}_{ij}^{In} = \frac{4}{d^{ev}} \begin{cases} \left[12\left(\frac{d^{ev}}{r_{ij}}\right)^{13} - 6\varepsilon\left(\frac{d^{ev}}{r_{ij}}\right)^{7}\right]\hat{\mathbf{r}}_{ij} & r_{ij} \geq 3 \\ \left[12\left(\frac{d^{ev}}{3}\right)^{13} - 6\varepsilon\left(\frac{d^{ev}}{3}\right)^{7}\right]\hat{\mathbf{r}}_{ij} & r_{ij} < 3 \end{cases} \tag{4}$$

where $\mathbf{r}_{ij} = \mathbf{r}_i - \mathbf{r}_j$, $r_{ij} = |\mathbf{r}_{ij}|$, $\hat{\mathbf{r}}_{ij}$ is the unit vector along $\mathbf{r}_{ij}$, and ε and d^{ev} are the energy and length parameters, respectively, whose values are addressed below.

The Brownian force is

$$\boldsymbol{F}_i^B = (\frac{6k_BT\zeta}{\Delta t})^{1/2}\boldsymbol{n} \tag{5}$$

where $\boldsymbol{n}$ is a random three-dimensional vector, each component of which is uniformly distributed in the interval $[1, -1]$.

In order to make sure the stability of the simulations even when two beads are overlapping with each other, the Lennard-Jones Potential is truncated. The truncation distance is chosen to produce the same level of maximum repulsive force as Larson's paper. [15]

2.2.3 Governing equations

The governing equations in the inertia free limit can be obtained by a force balance on each bead:

$$\boldsymbol{F}_i^D + \boldsymbol{F}_i^S + \boldsymbol{F}_i^{In} + \boldsymbol{F}_i^B = 0, i = 1,2, \dots, N \tag{6}$$

where the subscript i refers to the bead number and $\boldsymbol{F}_i^D$, $\boldsymbol{F}_i^S$, $\boldsymbol{F}_i^{In}$ and $\boldsymbol{F}_i^B$ are the hydrodynamic (viscous) drag force, the spring force (either FENE or harmonic), the bead-bead interaction force, and the Brownian force, respectively.

In the absence of hydrodynamic interaction (HI), the polymer chain is referred to be in the free draining (FD) limit. In order to consider the HI condition in determining dynamics for our model, the Rotne-Prager-Yamakawa (RPY) tensor was utilized. The disturbed velocity $\boldsymbol{v}_i'$, produced by another bead j, is a linear function of the hydrodynamic drag force $\boldsymbol{F}_j^D$,

$$\boldsymbol{v}_i^{'} = -\boldsymbol{\Omega}_{ij}\boldsymbol{F}_j^D = \boldsymbol{\Omega}_{ij}\left(\boldsymbol{F}_j^S + \boldsymbol{F}_j^{In} + \boldsymbol{F}_j^B\right) \tag{7}$$

where $\boldsymbol{\Omega}_{ij}$ is the hydrodynamic interaction tensor between two beads. Ermak and McCammon [17] showed that the disturbance velocity can be included into the Langevin equation by introducing the diffusion tensor,

$$\mathbf{D}_{ij} = \frac{k_B T}{\zeta}\left(\delta_{ij}\mathbf{I} + \zeta\boldsymbol{\Omega}_{ij}\right) \tag{8}$$

where δ_{ij} is the Kronecker delta.

The RPY tensor is given by [14,18,20]

$$\boldsymbol{D}_{ii} = \boldsymbol{I} \tag{9}$$

$$\boldsymbol{D}_{ij} = \frac{3}{4}\frac{a}{r_{ij}}\begin{cases}\left[\left(1+\frac{2a^2}{3r_{ij}^2}\right)\boldsymbol{I}+\left(1-\frac{2a^2}{r_{ij}^2}\right)\frac{\mathbf{r}_{ij}\mathbf{r}_{ij}}{r_{ij}^2}\right], & r_{ij}\geq 2a \\ \frac{r_{ij}}{2a}\left[\left(\frac{8}{3}-\frac{3r_{ij}}{4a^2}\right)\boldsymbol{I}+\frac{r_{ij}\mathbf{r}_{ij}\mathbf{r}_{ij}}{4a\ r_{ij}^2}\right], & r_{ij}<2a\end{cases} \tag{10}$$

A square root relationship exists between $\boldsymbol{D}_{ij}$ and $\boldsymbol{\sigma}_{ij}$, [20]

$$\boldsymbol{D}_j = \sum_{l=1}\boldsymbol{\sigma}_{il}\cdot\boldsymbol{\sigma}_{lj} \tag{11}$$

After substituting and rearranging, the stochastic differential equation including HI becomes,

$$\dot{\mathbf{r}}_i = (\nabla\mathbf{u})^T\mathbf{r}_i + \sum_{j=1}^{N}\frac{\mathbf{D}_{ij}\cdot\left(\boldsymbol{F}_j^S+\boldsymbol{F}_j^{BB}\right)}{k_B T} + \left(\frac{6}{\Delta t}\right)^{1/2}\sum_{j=1}^{i}\boldsymbol{\sigma}_{ij}\,\boldsymbol{n}_j \tag{12}$$

By applying dimensionless units, the governing equation is,

$$\mathbf{r}_i = \mathbf{r}_i^{old} + \left[(\nabla\boldsymbol{u})^T\cdot\mathbf{r}_i + \sum_{j=1}^{N}\boldsymbol{D}_{ij}\left(\boldsymbol{F}_j^S + \boldsymbol{F}_j^{BB}\right)\right]\Delta t + \sqrt{6\Delta t}\sum_{j=1}^{i}\boldsymbol{\sigma}_{ij}\,\boldsymbol{n}_j \tag{13}$$

where $\mathbf{r}_i$ and $\mathbf{r}_i^{old}$ are the position vectors of bead i at the new and old times respectively. Incorporating the interactions between surface and vWF multimer into the governing equations, it becomes,

$$\mathbf{r}_i = \mathbf{r}_i^{old} + \left[(\nabla \boldsymbol{u})^T \cdot \mathbf{r}_i + \sum_{j=1}^{N} \boldsymbol{D}_{ij} \left(\boldsymbol{F}_j^S - \boldsymbol{F}_{j-1}^S + \boldsymbol{F}_j^{BB} + \boldsymbol{F}_j^{Wall} + \boldsymbol{F}_j^{Bond}\right) + \sum_{j=1}^{N} \boldsymbol{\nabla_j} \cdot \boldsymbol{D}_{ij}\right]\Delta t + \sqrt{6\Delta t} \sum_{j=1}^{i} \boldsymbol{\sigma}_{ij}\, \boldsymbol{n}_j \quad (14)$$

The term $\boldsymbol{\nabla_j} \cdot \boldsymbol{D}_{ij}$ will compensate for the spurious flux due to inhomogeneities in the self-mobility. The tensor $\boldsymbol{\sigma}_{ij}$ is obtained from a Cholesky decomposition of $\boldsymbol{D}_{ij}$. In this thesis, only the free draining (FD) condition will be considered, thus the hydrodynamic interaction (HI) cases will not be taken into account.

2.3 Parameterization of vWF model

In the present work, due to the same model, all the parameters used in the vWF model were adopted from Ouyang's study [30]. The parameters of the FENE spring are H = $0.1428\, mN/m$ and $Q_0 = 60\ nm$. The radius of bead a = 10 nm, which is half of the length of the fully unfolded monomer (80 nm) minus the maximum extended length for the FENE spring Q_0. The length parameter in Lennard-Jones potential is $d^{ev} = 2a/2^{1/6}$ and the dimensionless energy parameter is ε = 1.43. Temperature is set to be T = 300 K. The length and force will be made dimensionless by scaling with$\sqrt{k_b T/H} = 5.3846\, nm$ and$\sqrt{Hk_b T} = 0.7692\, pN$, respectively. The drag coefficient is $\zeta = 6\pi\mu a$ =1.8848 × 10^{-10} $N \cdot s/m$ and the time scale is $\zeta/H = 1.319\, \mu s$. The dynamic viscosity μ of phosphate buffered saline solvent is almost the same as water, and is set to $1\ Ns/m^2$.

2.4 Simulation details

2.4.1 Criterion for diluteness of solvent

The "diluteness" plays a very important role in the polymer science. In a dilute polymer solution, the polymer concentration is low enough that the polymers do not interact with each other topologically or hydrodynamically. [21] As a result, it suggests that the effect of polymers on rheological properties of the fluid is linear. Either experimentally or theoretically, there always exist three concentration regimes: dilute, semi-dilute, and concentrated. [22] A general criterion for diluteness of a polymer solution is given by [21]

$$c < \frac{1}{[\eta]_0} \tag{15}$$

where $[\eta]_0$ is the intrinsic viscosity of the polymer in dilute solution and is defined as

$$[\eta]_0 = \lim_{c\to\infty} \frac{\eta-\eta_s}{c\eta_s} \tag{16}$$

where η is the solution viscosity and η_s is the viscosity of the solvent. The subscript "0" in $[\eta]_0$ means that it is measured at low flow rates. Once the solvent is sure to be dilute, the Brownian dynamics simulation can be simplified to exclude the interactions between different polymer chains like entanglements and only one vWF multimer needs to be initialized and taken into consideration during one simulation run.

2.4.2 vWF multimer initialization

In general, there are two different approaches that can be used to get the initial conformation of a single vWF multimer. The first method is to place the first bead at the origin, and subsequent beads at random directions and at certain fixed distance away from the beads preceding them, so as to obtain the initial conformation. Here, the initial

conformation was obtained by placing the first bead at the origin, and subsequent beads were placed either 4 or 5 dimensionless units away from the preceding beads, depending on whether the two beads were connected by a harmonic or FENE spring, respectively. The real position of placement was chosen randomly but to avoid overlaps with previously placed beads. In present simulation, 25 different initial conformations were initialized in different runs in order to improve statistics.

2.4.3 Quantity of interest

The radius-of-gyration was used to characterize the conformation of a vWF multimer and is defined as

$$R_g = \sqrt{\frac{\langle \sum_{i=1}^{N} |\mathbf{r}_i - \mathbf{r}_{c,m}|^2 \rangle}{N}} \tag{17}$$

where $\mathbf{r}_i$ is the position of ith bead, $\mathbf{r}_{c,m}$is the center position of mass of the chain and $\langle \cdot \rangle$ denotes an ensemble average.

The length of FENE springs is of great interests in this thesis because of its important physical and biological meaning, which needs to be quantified by averaging over all FENE springs in all vWF chains after the simulation reaches equilibriums.

2.4.4 Choosing time-steps

The selection of time-step Δt was dependent on whether the model was run with or without hydrodynamic effect. For free draining (FD) case, the simulations were conducted using the time-step of $\Delta t = 10^{-4}$. In the present study, only free draining case (FD) is considered. For extensional flow, the selection of time-step Δt is dependent on the accuracy and efficiency of our calculation. As it is discussed earlier, the simulations here were conducted using the time-step of either $\Delta t = 10^{-4}$ or $\Delta t = 10^{-5}$.

Meanwhile, another factor, which is whether the Lennard-Jones pairwise interaction is applied between beads or not, needs to be considered. Fig. 2.4.1 shows the differences among these situations.

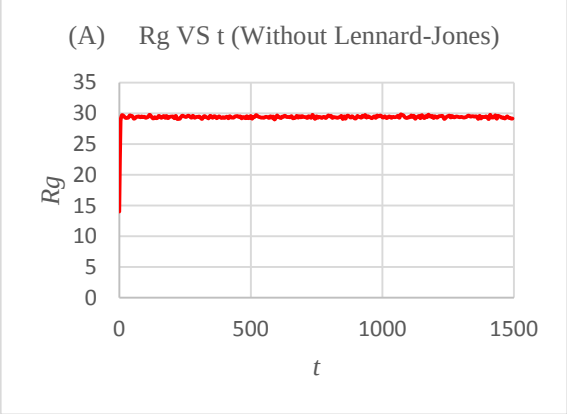

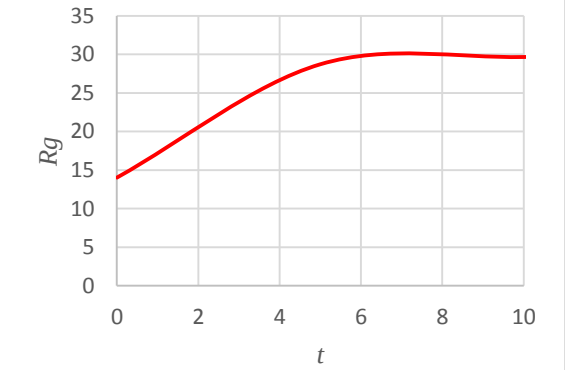

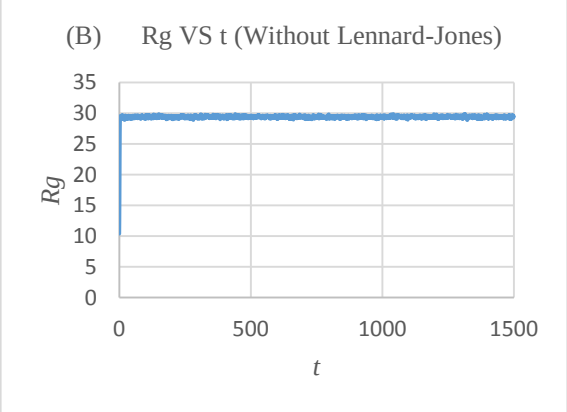

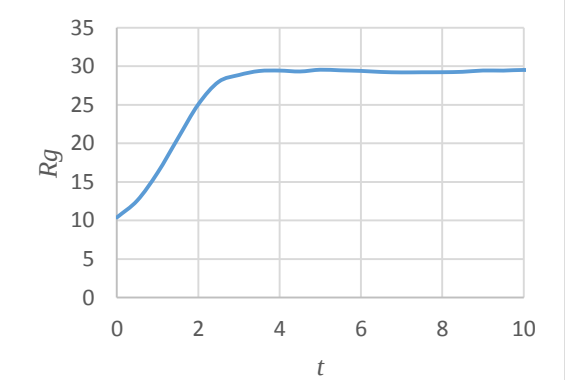

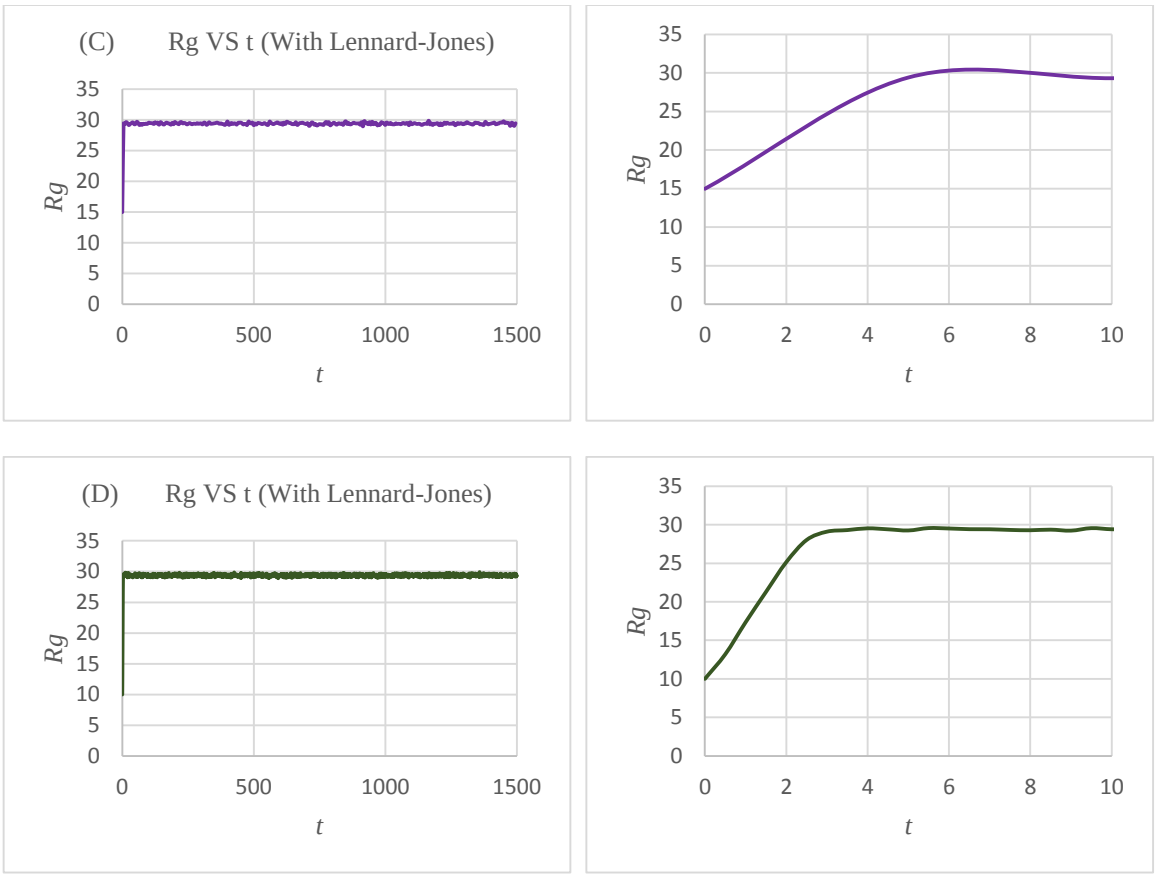

Fig. 2.4.1 *Rg* is plotted as a function of time for a 20-beads chain without HI when *Wi*=10 for four cases. (A) $\Delta \boldsymbol{t} = \mathbf{10^{-4}}$ without Lennard-Jones interaction, (B) $\Delta \boldsymbol{t} = \mathbf{10^{-5}}$ without Lennard-Jones interaction, (C) $\Delta \boldsymbol{t} = \mathbf{10^{-4}}$ with Lennard-Jones interaction, and (D) $\Delta \boldsymbol{t} = \mathbf{10^{-5}}$ with Lennard-Jones interaction.

The nominal value of the *Rg* obtained by both time steps are nearly the same with and without the Lennard-Jones pairwise interaction. This assures that temporal convergence is attained for the time step of $\Delta t = 10^{-4}$.

As a result, considering the computer configurations such as CPU, RAM, and the computational efficiency, the time-step of $\Delta t = 10^{-4}$ is sufficient to conduct simulations here.

2.4.5 Transient effects and equilibrium state

It is concluded that the time-step of $\Delta t = 10^{-4}$ satisfies the condition for temporal convergence. What is needed next is to determine if the whole time period is long enough to calculate the nominal value of the radius-of-gyration (*Rg*) accurately. Thus, using the time-step of $\Delta t = 10^{-4}$, for both situations whether the Lennard-Jones pairwise interaction is applied or not, the radius-of-gyration (*Rg*) is calculated as a function of time and is plotted in Fig. 2.4.2.

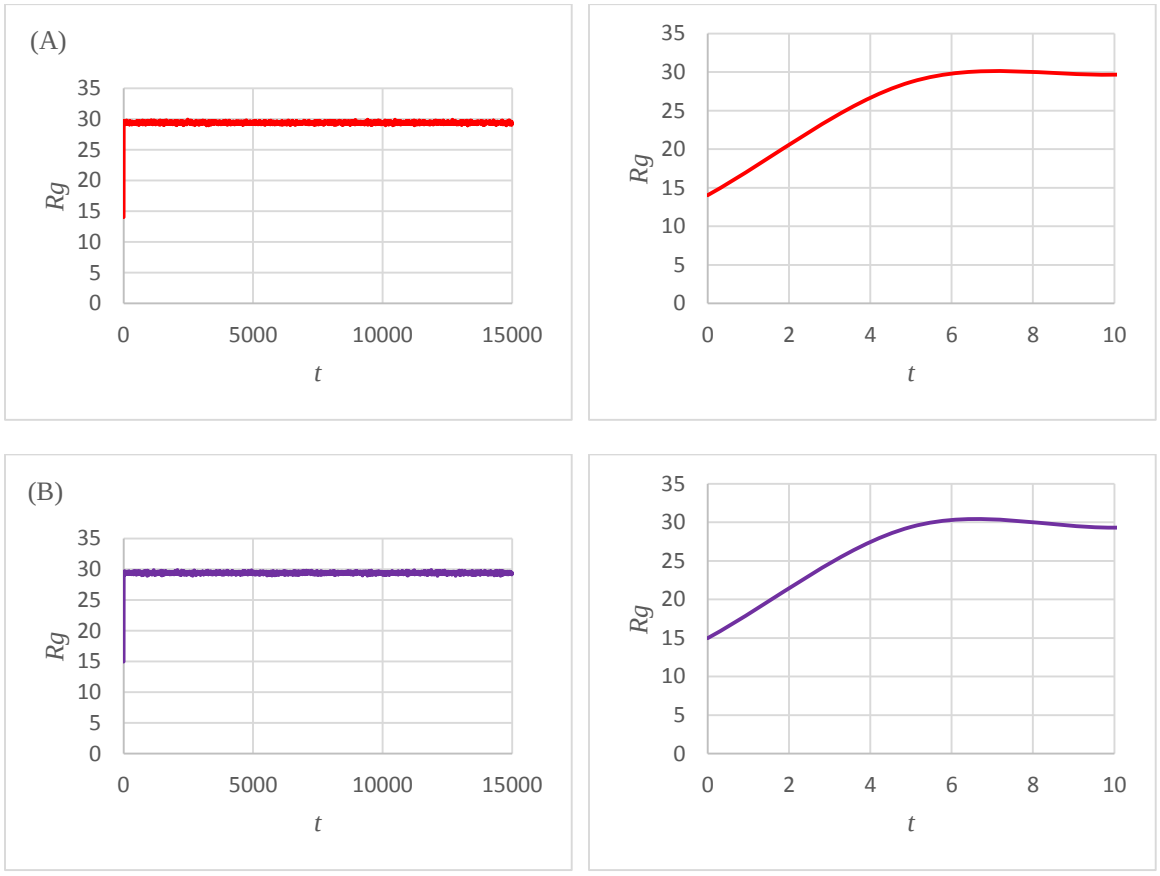

Fig. 2.4.2 *Rg* is plotted as a function of time for a 20-beads chain without HI when *Wi*=10 for two cases. (A) without Lennard-Jones pairwise interaction and (B) with Lennard-Jones pairwise interaction.

Following conclusions are reached:

1. The transition from initial configuration to the quasi equilibrium configuration is very short.
2. After the initial transition a stable equilibrium state is reached in both cases (with and without particle interaction).
3. The amplitude of the fluctuations in the equilibrium state is very small.

It is illustrated that there are no remarkable difference in the nominal value of radius-of-gyration of polymer chain between the existence and nonexistence of the Lennard-Jones potential interaction. Therefore, in order to simplify the simulations, this factor will not be considered in later study.

Moreover, the total computational time for simulation is long enough to reach quasi-equilibrium state and obtain accurate representation of the nominal values of the radius-of-gyration. As for the nominal value, in order to eliminate the influence transitional effects after the initialization of the vWF multimer, the average value of the radius-of-gyration is determined using the time window taken after the equilibrium state is reached. The sensitivity of the selection of time window for calculation of the nominal value of the radius of gyration is tested using different time period and different stage of the equilibrium state. It is shown that the nominal value of the radius of gyration predicted is not very sensitive to the averaging process.

2.4.6 Flow condition

The vWF multimers are modeled in quiescent solvent or in fluid flow. Since the study on shear flow condition has already been accomplished by other researchers in this group, only one flow condition will be investigated in this thesis: extensional flow. For a pure extensional flow, the velocity gradient of the flow field was given by

$$\nabla \mathbf{u} = \begin{pmatrix} \dot{\varepsilon} & 0 & 0 \\ 0 & -\frac{\dot{\varepsilon}}{2} & 0 \\ 0 & 0 & -\frac{\dot{\varepsilon}}{2} \end{pmatrix} \tag{17}$$

and $\dot{\varepsilon}$ is the extensional rate.

Chapter 3 Flow-induced conformation changes of homopolymers

3.1 Introduction

In order to get a better understanding of vWF's behaviors, a collapsed homopolymers in an infinite medium under the influence of fluid flow is considered. The conformational transition from coiled states to stretched states has been widely studied in the area of polymer science for many years. [19,23–25] D. Smith has successfully observed the movement of individual, flexible polymers in both steady shear and extensional flow by the use of video fluorescence microscopy and simulated single DNA molecule under these flow conditions, in which quantitative agreement has been achieved. Subsequently, R. Larson further developed the simulation methodology by considering self-entanglements. [14,26] The present results constitute a broad context, regarding conformational changes of homopolymers in response to various fluid flow types with or without various effects. In the present work, only extensional flow condition for the free draining (FD) cases is considered.

3.2 Results and discussion

The starting point of the present work is to consider vWF multimer in an infinite medium under the influence of extensional flows. [30] Basic approaches and the principles of the present model are based on those introduced by investigations from our research group. Interaction with surfaces and walls are not studied in the present work.

3.2.1 Calculation of the longest relaxation time

The Weissenberg number *Wi* is defined as the ratio of a viscoelastic fluid's relaxation time τ to some characteristic temporal scale. In simple extensional flow,

$$Wi = \tau\dot{\varepsilon} \tag{18}$$

where $\dot{\varepsilon}$ is extentional rate. The longest relaxation time τ of vWF multimers varies with the number of repeat units, which means the number of monomers in present study. The number of monomers is *N*/2, since *N* is the number of beads. [30] With the effort of researchers in our group, the method of obtaining relaxation curves was obtained, and then we just need to directly refer to the relaxation curves for square of end-to-end distance versus time for *N* = 60 vWF multimers, which is shown in Fig. 3.2.1 [30]. From this figure, it suggests the longest relaxation time τ was only measured when the ratio of end-to-end distance to *L* is below 0.3. [16,27] Simulations with three different initial conformations were conducted for the same number of beads. However, results from all the simulations were essentially identical, which demonstrates that the initial conformation of vWF multimer has little influence on τ.

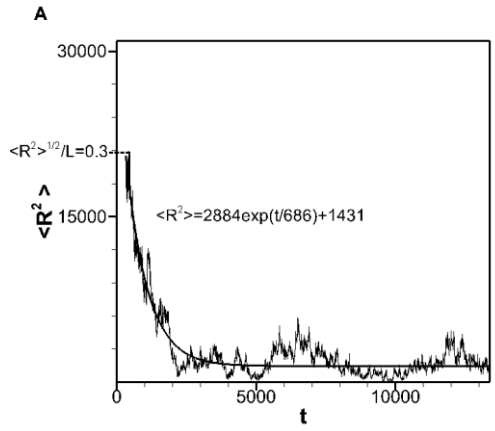

Fig. 3.2.1 Relaxation curves for square of end to end distance versus time using 60 beads without HI [30]

In addition, according to previous study in our group, Fig. 3.2.2 shows the longest relaxation time τ for different number of beads with and without HI, of which only the results for free draining (FD) cases are considered in present work. [28] It suggests that a power-law scaling of relaxation time with number of beads exists, with exponents of 1.97 in the simulation for FD cases. The R^2 values showing the quality of the fits are 0.9929 for FD, while the exponents determined here agree well with the Rouse relaxation time (without HI) $\tau_R \sim N^2$, which is predicted by polymer theory. [29]

Considering the molecular size used in the present FD simulations, prediction for the relaxation time differs from experimental observation by nearly a factor of two. Due to the simplicity of our model, our prediction is rational. Therefore, it can be taken as an indication that the relaxation time here is more appropriately predicted in FD cases.

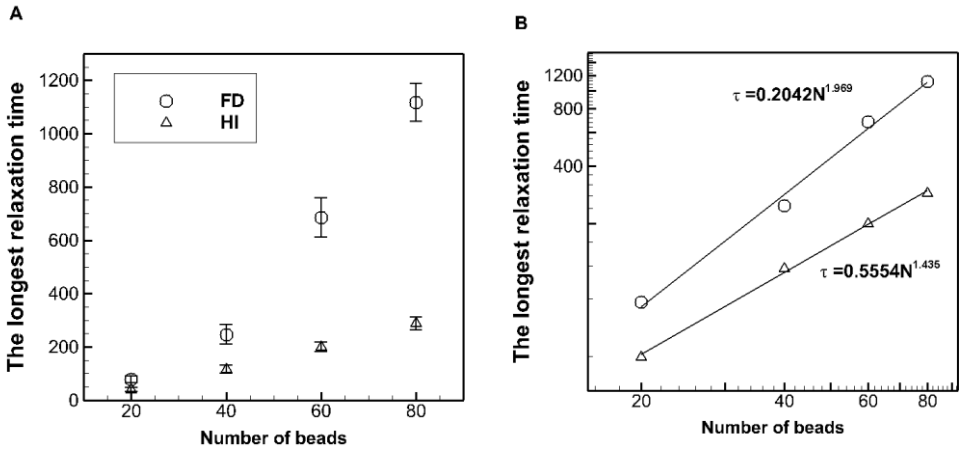

Fig. 3.2.2 Dependence of the longest relaxation time $\boldsymbol{\tau}$ on the number of beads *N* with and without hydrodynamics: (A) linear scale plot with error bar (confidence interval) and (B) log scale plot.

3.2.2 The effect of Lennard-Jones pairwise interaction

The radius-of-gyration of the 20-bead chain is determined for unfolding process for a wide range of Weissenberg numbers (*Wi*) in response to extensional flows with or without Lennard-Jones pairwise interaction, so as to understand the effect of this principle potential interaction on the conformation of vWF multimers.

Nominal values of the radius-of-gyration for different values of Weissenberg numbers are listed in Table 3.2.1.

Table 3.2.1 Nonimal values of *Rg* for different values of *Wi*

Weissenberg Number	*Rg* (without Lennard-Jones)	*Rg* (with Lennard-Jones)
0	7.07	8.95
0.1	13.26	15.82
0.5	20.16	22.16
1	22.38	22.47
10	29.34	30.18
50	58.16	61.16
100	62.03	62.66
200	63.40	63.51

Fig. 3.2.3 depicts the corresponding nominal values of the radius-of-gyration as a function of the Weissenberg number with and without the Lennard-Jones potential interaction.

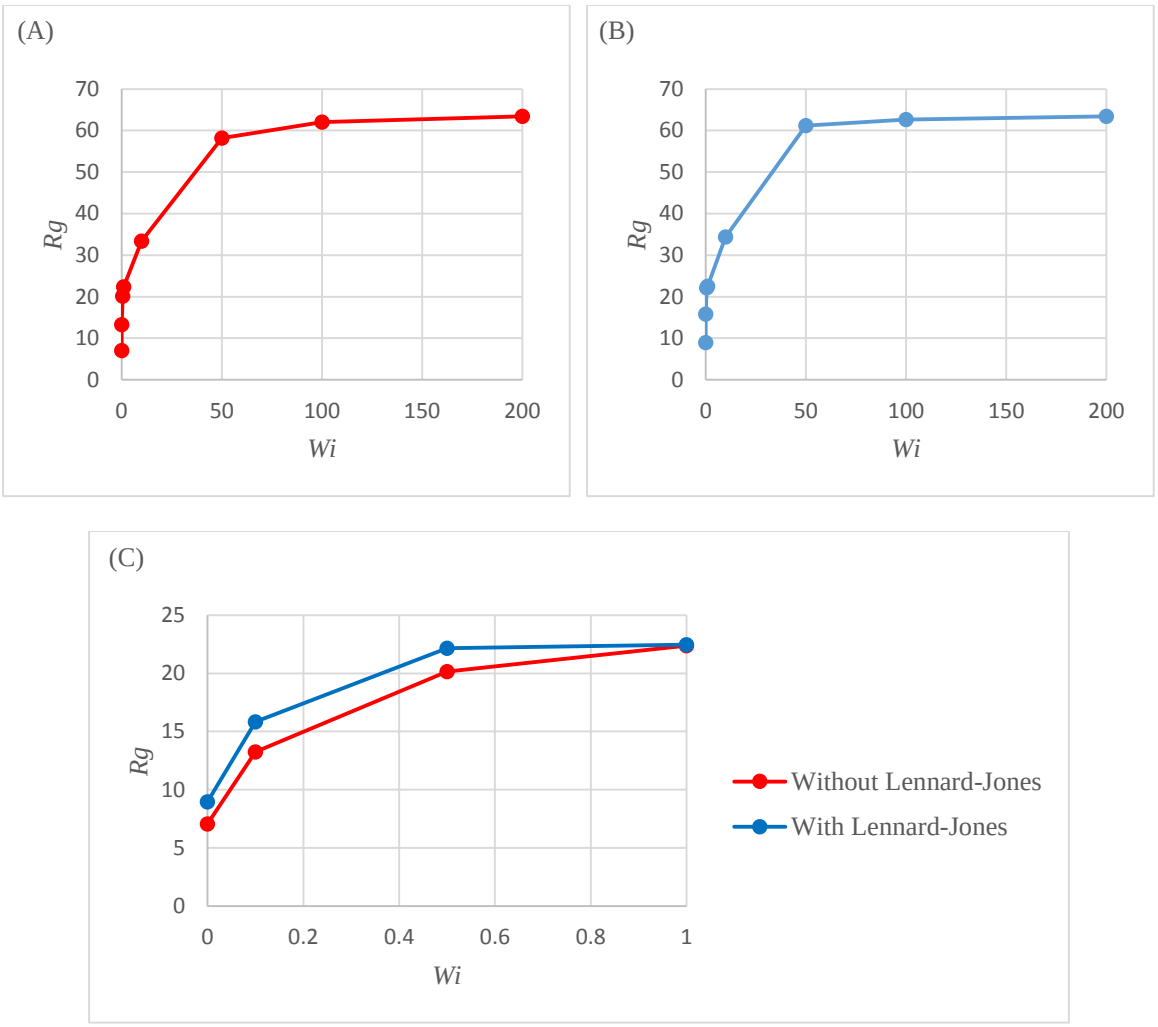

Fig. 3.2.3 Dependence of the radius-of-gyration (*Rg*) on Weissenberg number (*Wi*) for two cases. (A) without Lennard-Jones pairwise interaction, (B) with Lennard-Jones pairwise interaction and (C) details comparison between two situations.

It is demonstrated that the bead-bead interaction influences the vWF conformation only at low values of Weissenberg number. The radius of gyration with bead-bead interaction becomes nearly the same as that without bead-bead interaction as the Weissenberg number reaches unity or above. With increasing intensity of extensional flows, bead-bead interaction becomes less influential.

Bead-bead interaction has some degree of influence at low value of Weissenberg number.

This is due to the repulsive forces. In the limit of low extensional flows, small values of the Weissenberg number, the radius-of-gyration in the equilibrium state is not large enough so that beads are closer to each other and the amplitude of the repulsive forces are larger. Repulsive forces in such limit leads to larger degree of the unfolding of the vWF multimer. However, when the Weissenberg number reaches unity or above, this can be viewed as a critical intensity level for the onset of unfolding induced by extensional flows, the vWF multimer chain extends and repulsive forces lose their dominance. Therefore, for values of *Wi* above near and above unity, the radius-of-gyration (*Rg*) becomes nearly independent of the Lennard-Jones pairwise interaction between beads.

Since the effect of the Lennard-Jones pairwise interaction on the conformational changes of the vWF multimer is only significant for small extension rates or small values of Weissenberg number, the Lennard-Jones bead-bead interaction is neglected in all simulation presented in this document.

3.2.3 Calculation of molecular response in extensional flows

Previous study shows the dependence of radius-of-gyration on the length of vWF multimer in a no-flow condition (FD simulations), as shown in Fig. 3.2.4. [30] The results presented in Fig. 3.2.4 is performed using model parameters determined from experimental observations as mentioned above. Ouyang and his co-workers [30] has already successfully showed that *Rg* of vWF scales with $N^{0.322}$.

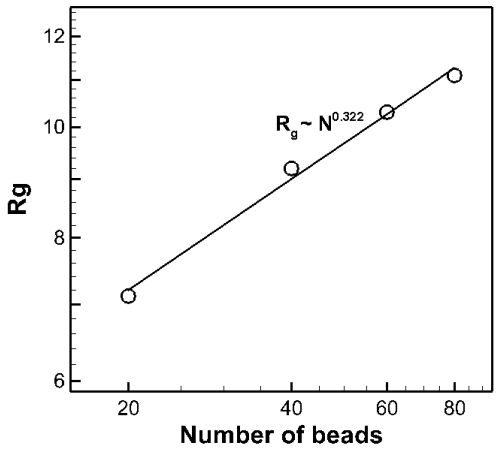

Fig. 3.2.4 Dependence of the radius-of-gyration *Rg* on chain length *N*. [30]

Temporal characteristics for a single 20 beads vWF multimer under no flow (*Wi* = 0) and in extensional flows with *Wi* = 0.1, *Wi* = 1 and *Wi* = 10 are depicted in Fig. 3.2.5. When vWF is subject to strong extensional flows (*Wi* = 10), the vWF multimer reacted rapidly to the extensional flow such that there is no apparent transient state. In that case, the ensemble average of *Rg* was calculated by averaging all data during a simulation run. For 20-bead vWF multimer, the simulation yielded an ensemble average *Rg* = 29.34. The vWF multimer is significantly uncoiled at this flow condition, which can enable the A3 domain to bind to the collagen. Compared to the *Wi* = 10 case, the vWF multimer exhibits less degree of unfolding and overall larger fluctuations in the *Wi* = 1 case, in which the assemble average *Rg* = 23.28. However, occasional significant unfolding of vWF multimers still occurs at this relatively weak extensional flow. This emphasizes the strong sensitivity of our model vWF molecules to the extensional flow condition. Where there is no flow, the assemble average *Rg* = 7.62. Relatively large fluctuations even persist in the no-flow case, consistent with the vWF polymer forming a compact globule, as illustrated in Fig. 3.2.5.

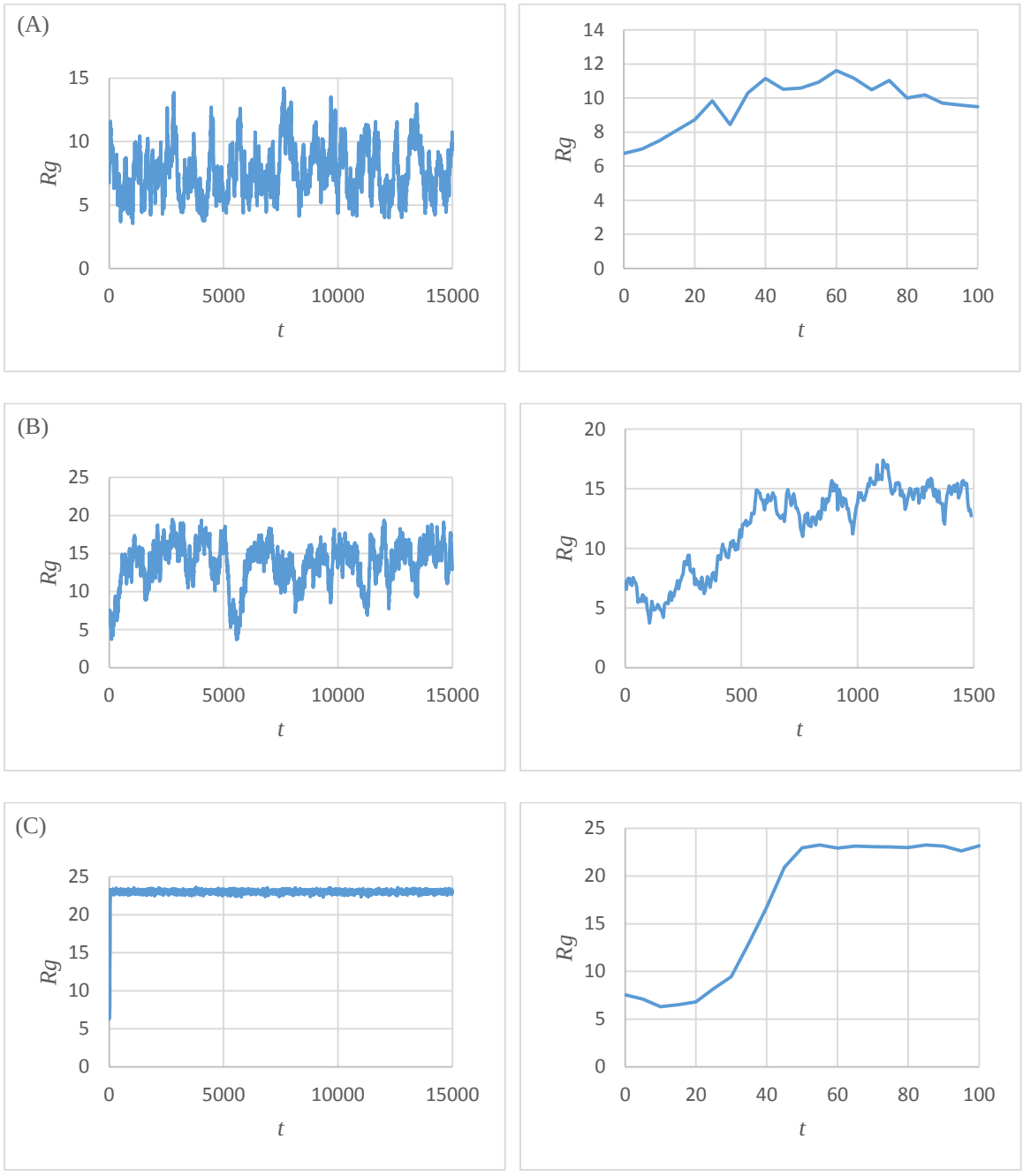
(A)
Rg
t
0
5
10
15
0
5000
10000
15000
Rg
t
0
2
4
6
8
10
12
14
0
20
40
60
80
100
(B)
Rg
t
0
5
10
15
20
25
0
5000
10000
15000
Rg
t
0
5
10
15
20
0
500
1000
1500
(C)
Rg
t
0
5
10
15
20
25
0
5000
10000
15000
Rg
t
0
5
10
15
20
25
0
20
40
60
80
100

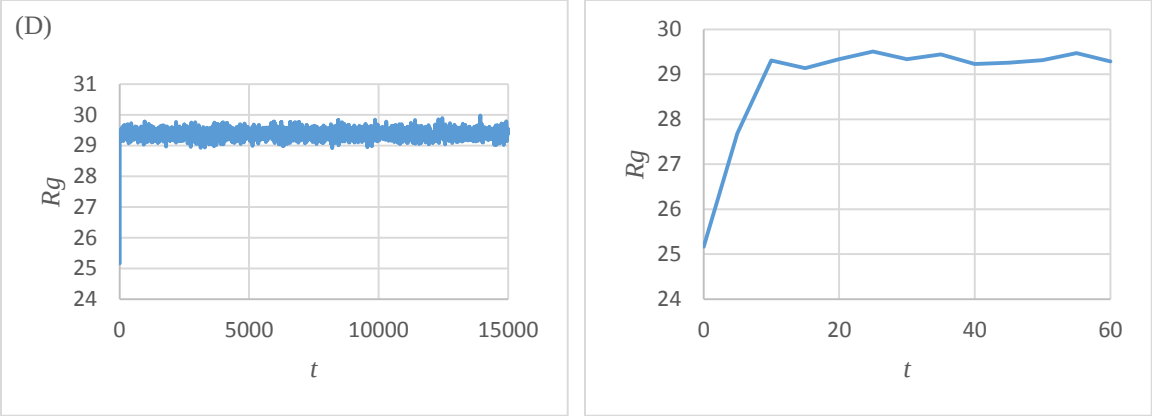

Fig. 3.2.5 Time dependence for 20-bead chain: (A) no flow, (B) *Wi*=0.1, (C) *Wi*=1 and (D) *Wi*=10.

Moreover, Fig. 3.2.6, 3.2.7, 3.2.8 and 3.2.9 show stages of conformational changes of 20 beads vWF multimers in FD case for no flow, *Wi* = 0.1, *Wi* = 1 and *Wi* = 10, respectively. The results indicate that as the unfolding process becomes faster and more thoroughly as extension rate increases.

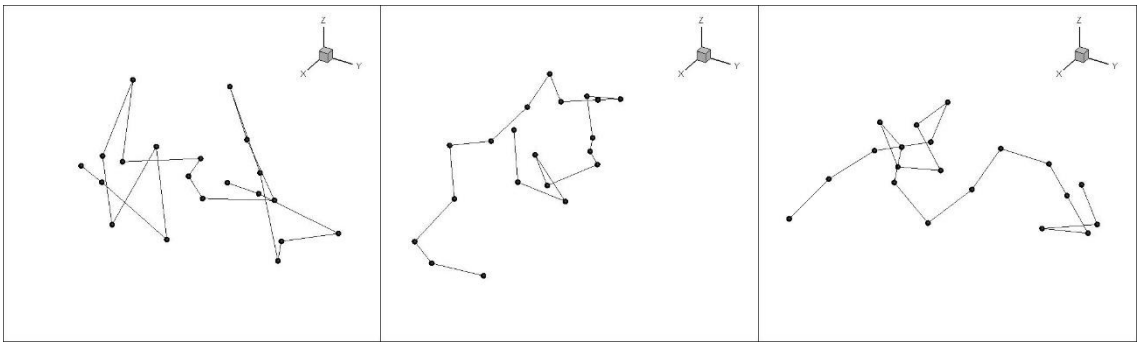

Fig. 3.2.6 Snapshots of polymer configuration illustration for various stages during unfolding process for no flow case: (A) start, (B) middle and (C) end.

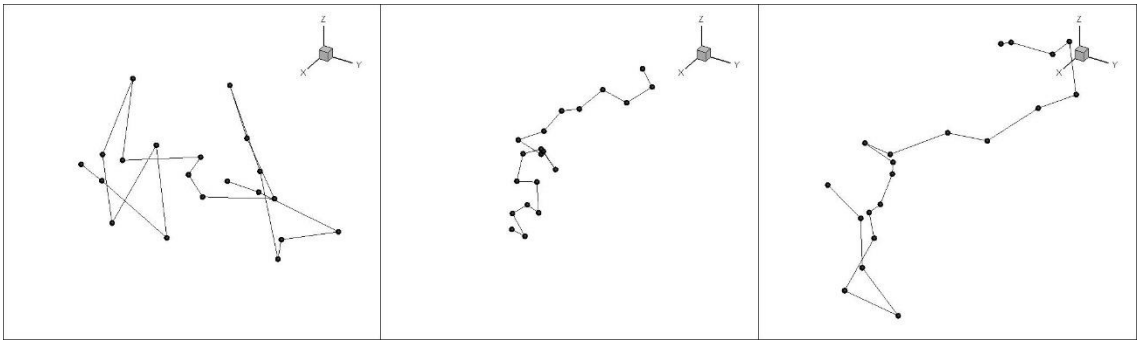

Fig. 3.2.7 Snapshots of polymer configuration illustration for various stages during unfolding process for *Wi*=0.1 case: (A) start, (B) unfold and (C) end.

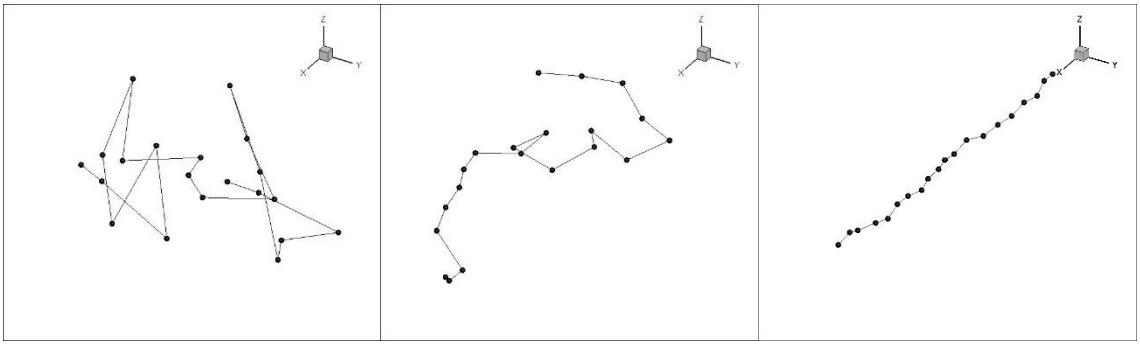

Fig. 3.2.8 Snapshots of polymer configuration illustration for various stages during unfolding process for *Wi*=1 case: (A) start, (B) unfold and (C) end.

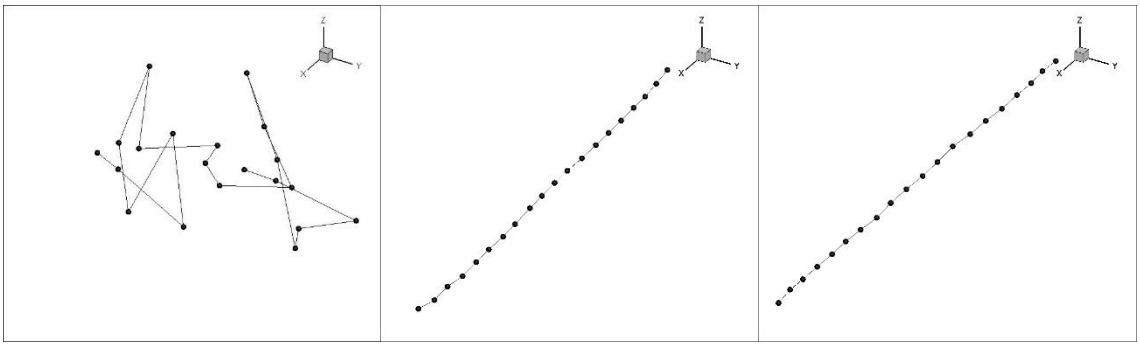

Fig. 3.2.9 Snapshots of polymer configuration illustration for various stages during unfolding process for *Wi*=10 case: (A) start, (B) unfold and (C) end.

3.2.4 The effect of extensional flows – different size of vWF multimer

The effect of the intensity of extensional flows on the conformation of vWF multimer can be investigated when the Lennard-Jones pairwise interaction is neglected. 20-bead vWF multimer is considered in these simulations. The nominal value of *Rg* are listed in Table 3.2.2 for a wide range of *Wi*, which is varied from 0 to 200, while *Wi*=200 is representing very strong extensional flows.

Table 3.2.2 Nominal values of *Rg* for a wide range of *Wi*

Weissenberg Number	*Rg*	Weissenberg Number	*Rg*
0	7.07	0.4	18.75
0.01	7.22	0.5	20.16
0.02	7.25	1	22.38
0.03	7.34	10	29.34
0.05	7.64	20	40.74
0.07	8.84	30	48.77
0.08	9.24	40	54.19
0.09	10.02	50	58.16
0.1	13.26	100	62.03
0.2	14.83	200	63.40
0.3	16.52		

Fig. 3.2.10 depicts the nominal values of radius-of-gyration as a function of the Weissenberg number. From the linear plot, it indicates that, as Weisennberg number increases, the radius-of-gyration increase rapidly at the beginning when Weisennberg number is small. Then the increase of radius-of-gyration slows down and eventually reach an equilibrium state.

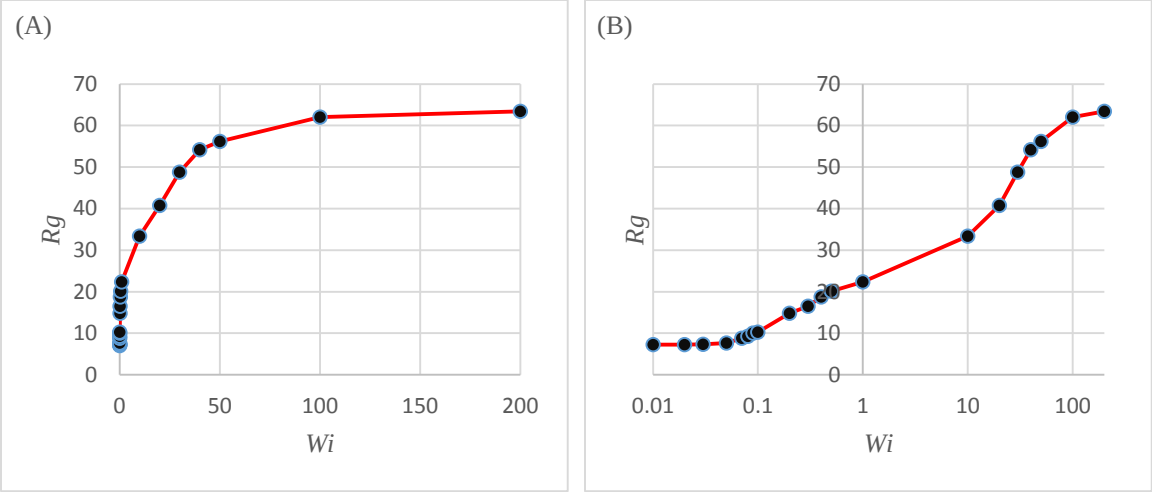

Fig. 3.2.10 Dependence of the radius-of-gyration (*Rg*) for 20-bead chain on Weissenberg number (*Wi*) (A) linear scale plot and (B) log scale plot.

Simulations are conducted for different size of vWF multimers subject to extensional flows. 20, 40, and 60 beads vWF multimers are used in these simulations. The nominal value of *Rg* as a function of *Wi* is plotted in Fig. 3.2.11. The nominal value of *Rg* normalized by $N^{0.322}$ of 25 different randomly initialized vWF multimers for each vWF multimer chain. Different random number starting seeds and configurations are used in simulations. As expected, normalized *Rg* monotonically increases with *Wi* and then approaches an apparent asymptote, regardless of the length of the vWF multimer. This behavior is similar to that documented by Larson, *et al*. [15,24] Normalized *Rg* are approximately the same for all cases when *Wi* is below 0.05; in this limit of extremely low extensional flows, data for all cases shows little dependence on *Wi*. For *Wi* > 0.05 normalized *Rg* increases as the length of the vWF is increased. In addition, the difference in the normalized *Rg* increases further as *Wi* increases, as shown in Fig. 3.2.11. This is because longer vWF multimers have a greater number of dynamic structural modes through which they interact with imposed flow fields. Thus, longer molecules have more potential to unfold and are more sensitive

to high rate extensional flow conditions.

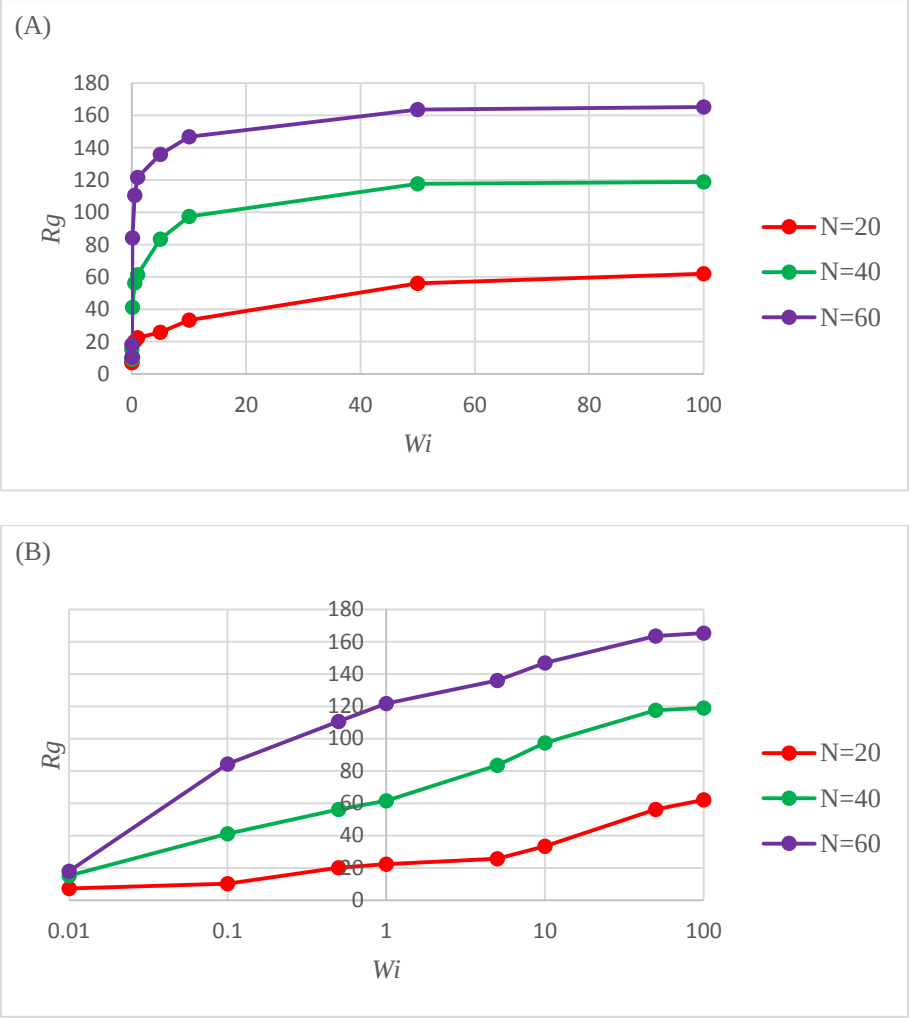

Fig. 3.2.11 Dependence of the radius-of-gyration (*Rg*) for different length of chains on Weissenberg number (*Wi*): (A) linear scale plot and (B) log scale plot.

The length of vWF multimer has a profound influence on characteristics of vWF multimer under extensional flows. Longer vWF chains have been shown to have more potential to unfold; this tendency becomes increasingly apparent for higher extensional flows, which helps to explain the observed dependence of vWF functionality on the molecular size.

3.2.5 Comparison with unfolding behaviors in response to shear flow

As previous studies show, the intensity of induced-flow, no matter shear flow or extensional flow, does have an impact on the unfolding behaviors of vWF multimers. However, the characteristics of unfolding can be different for these flow types. For shear flow, the radius-of-gyration will not increase until Weissenberg number reaches unity, which suggests that only after the intensity of induced flow reaches a critical value (For example, Wi=1), the unfolding process will start. On the other hand, for extensional flows, the radius-of-gyration starts increasing even when Weissenberg number is as low as 0.05, which suggests extensional flows have stronger influence on unfolding of vWF multimers.

In summary, vWF multimers unfolds more in extensional flows than in shear flows. Also, comparing with shear flows, the transitional stage of the vWF multimer unfolding subjects to the extensional flows is much shorter. Extensional flows causes larger degree of unfolding and smaller amplitude of fluctuations in conformation of vWF.

3.3 Conclusion

The new model was used to study the conformational changes under various intensity of extensional flow for vWF multimers. Flow intensity and molecular size do have profound influences on the behavior characteristics of vWF multimer unfolding process. A longer chain vWF has been shown to unfold much faster in response to stronger extensional flows. Besides, longer vWF chains have potential to unfold larger extend, which becomes increasingly apparent for high extensional flows. These observations help to explain some observed dependence of vWF functionality on hydrodynamic forces and the molecular size.

Chapter 4 Summary

von Willebrand Factor is one of the dominant responders in blood clotting process. While at high flow rates, vWF becomes requisite because the platelets in vessels no longer maintain a sufficient level of adhesion at the surface to form blood clots. [5,7,30] In this case, vWF is proven to implement various functionalities: the A3 domain on vWF binds to collagen at the surface of the extracellular matrix and vWF interact with platelets. Due to the various domains, vWF has an extremely complicated structure. Specifically, Zhang, *et al.* [12] has ever used single molecule force spectroscopy method to show the inner structure and mechanical characteristics of a vWF monomer's domains. Their work pointed out that the A2 domain of vWF, which lacks protection by disulfide bonds, could be unfolded with applied forces which may indeed produce under very rapid blood flow conditions. Furthermore, in comparison with the size of a non-extended monomer, the A2 domain demonstrates a large degree of elongation while unfolding. A novel vWF model which aims to more realistically describe this molecular structure is presented in this thesis. Particularly, the model is able to capture the primary mechanical response of a single monomer, which is accomplished by modeling vWF monomers as an extensible domain with relatively rigid domains on either side of it. The A2 domain has been proven to undergo significant unfolding during single molecule stretching experiments. [12] The extensible domains on a vWF monomer are modeled as a FENE spring, which is capable of significant extension. At each end of the spring is a spherical bead to represent neighboring rigid domains. Adjacent monomers are connected by a relatively stiff harmonic spring between beads on each monomer, so as to form the vWF multimers of desired length.

Based on the studies of previous scholars, the present thesis extended the context of vWF behaviors to another level of complexity-the response to extensional flow. Here we started with considering certain homopolymers under the influence of extensional flows, where vWF multimer adhesion to the collagen-coated surfaces is neglected. After selecting the appropriate time step and time period via optimization (computer configuration, computation efficiency, etc.), it requires to investigate the effect of the existence of Lennard-Jones potential interaction and the dependence of radius-of-gyration of the vWF multimer under unfolding on both time, Weissenberg numbers and chain length.

As a result, in comparison with cases without Lennard-Jones pairwise interaction, the application of Lennard-Jones pairwise interaction between beads does generate bigger radius-of-gyration in response to low extension rates, which is caused by repulsion force. In the limit of low extension rates, which means the Weissenberg number is small, the radius-of-gyration for equilibrium state is not big enough and repulsion force dominates, so that it increases the radius-of-gyration of the conformational changes of vWF multimer. However, after Weissenberg number reaches unity, vWF multimer chain will unfold thoroughly and repulsion force will lose its dominance rule. Therefore, the equalization of the radius-of-gyration in both situations becomes apparent for higher flows but only above the critical Weissenberg number of unity.

Furthermore, molecular length does have a profound influence on characteristics of vWF multimer under extensional flows. It has been predicted that longer vWF chains have more

potential to unfold; this tendency becomes increasingly apparent in higher extensional flows. This prediction helps to explain some of the observed dependence of vWF functionality on the molecular size. On the other hand, flow types do have different influences on the unfolding behaviors of vWF multimers. For shear flow, the unfolding process starts at higher shear rates as Weissenberg number becomes greater than one. While for extensional flows, the unfolding process will apparently start when Weissenberg number reaches above 0.05-0.07, which indicates the vWF umltimer unfolding is more sensitive to extensional flow. Therefore, the vWF multimer under extensional flow will undergo a stronger and faster unfolding process than shear flow.

The results predicted here reflect the dynamic conformation of vWF in response to extensional flows, and they will help to understand the molecular mechanisms underlying vWF functionality. Moreover, these discoveries will also make contribution to understand the causes of vWF related diseases and provide important inspirations for disease diagnosis and therapeutics.

Bibliography

[1] M.D. Wang, Manipulation of single molecules in biology., Curr. Opin. Biotechnol. 10 (1999) 81–6.

[2] L.H. Sperling, INTRODUCTION TO PHYSICAL POLYMER, n.d.

[3] S.F. De Meyer, B. De Maeyer, H. Deckmyn, K. Vanhoorelbeke, Von Willebrand factor: drug and drug target., Cardiovasc. Hematol. Disord. Drug Targets. 9 (2009) 9–20.

[4] J.E. Sadler, BIOCHEMISTRY AND GENETICS, (1998) 395–424.

[5] T.A. Springer, Review Article von Willebrand factor , Jedi knight of the bloodstream, 124 (2014) 1412–1425. doi:10.1182/blood-2014-05-378638.Helical.

[6] et al Nigel Key, Michael Makris, Practical Hemostasis and Thrombosis, 2009.

[7] Z.M. Ruggeri, Von Willebrand factor: looking back and looking forward., Thromb. Haemost. 98 (2007) 55–62. doi:10.1160/TH07.

[8] H.E. Gerritsen, R. Robles, B. La, Plenary paper Partial amino acid sequence of purified von Willebrand factor – cleaving protease, 98 (2001) 1654–1661.

[9] G.G. Levy, W.C. Nichols, E.C. Lian, T. Foroud, J.N. McClintick, B.M. McGee, et al., Mutations in a member of the ADAMTS gene family cause thrombotic thrombocytopenic purpura., Nature. 413 (2001) 488–94. doi:10.1038/35097008.

[10] K. Soejima, N. Mimura, M. Hirashima, H. Maeda, T. Hamamoto, T. Nakagaki, et al., A novel human metalloprotease synthesized in the liver and secreted into the blood: possibly, the von Willebrand factor-cleaving protease., J. Biochem. 130 (2001) 475–80.

[11] X. Zheng, D. Chung, T.K. Takayama, E.M. Majerus, J.E. Sadler, K. Fujikawa, Structure of von Willebrand factor-cleaving protease (ADAMTS13), a metalloprotease involved in thrombotic thrombocytopenic purpura., J. Biol. Chem. 276 (2001) 41059–63. doi:10.1074/jbc.C100515200.

[12] X. Zhang, K. Halvorsen, C.-Z. Zhang, W.P. Wong, T. a Springer, Mechanoenzymatic cleavage of the ultralarge vascular protein von Willebrand factor., Science. 324 (2009) 1330–4. doi:10.1126/science.1170905.

[13] B. Nieswandt, C. Brakebusch, W. Bergmeier, V. Schulte, D. Bouvard, R. Mokhtari-Nejad, et al., Glycoprotein VI but not alpha2beta1 integrin is essential

for platelet interaction with collagen., EMBO J. 20 (2001) 2120–30. doi:10.1093/emboj/20.9.2120.

[14] A. Alexander-Katz, M. Schneider, S. Schneider, A. Wixforth, R. Netz, Shear-Flow-Induced Unfolding of Polymeric Globules, Phys. Rev. Lett. 97 (2006) 138101. doi:10.1103/PhysRevLett.97.138101.

[15] N. Hoda, R.G. Larson, Brownian dynamics simulations of single polymer chains with and without self-entanglements in theta and good solvents under imposed flow fields, J. Rheol. (N. Y. N. Y). 54 (2010) 1061. doi:10.1122/1.3473925.

[16] C.-C. Hsieh, L. Li, R.G. Larson, Modeling hydrodynamic interaction in Brownian dynamics: simulations of extensional flows of dilute solutions of DNA and polystyrene, J. Nonnewton. Fluid Mech. 113 (2003) 147–191. doi:10.1016/S0377-0257(03)00107-1.

[17] D.L. Ermak, J.A. McCammon, Brownian dynamics with hydrodynamic interactions, J. Chem. Phys. 69 (1978) 1352. doi:10.1063/1.436761.

[18] R.M. Jendrejack, M.D. Graham, J.J. De Pablo, Hydrodynamic interactions in long chain polymers: Application of the Chebyshev polynomial approximation in stochastic simulations, J. Chem. Phys. 113 (2000) 2894. doi:10.1063/1.1305884.

[19] J.S. Hur, E.S.G. Shaqfeh, R.G. Larson, Brownian dynamics simulations of single DNA molecules in shear flow, J. Rheol. (N. Y. N. Y). 44 (2000) 713. doi:10.1122/1.551115.

[20] R.M. Jendrejack, J.J. De Pablo, M.D. Graham, Stochastic simulations of DNA in flow: Dynamics and the effects of hydrodynamic interactions, J. Chem. Phys. 116 (2002) 7752. doi:10.1063/1.1466831.

[21] R.G. Larson, The rheology of dilute solutions of flexible polymers: Progress and problems, J. Rheol. (N. Y. N. Y). 49 (2005) 1. doi:10.1122/1.1835336.

[22] M. Bercea, C. Ioan, S. Ioan, B.C. Simionescu, C.I. Simionescu, Ultrahigh molecular weight polymers in dilute solutions, 1999. doi:10.1016/S0079-6700(99)00007-6.

[23] P.S. Doyle, E.S.G. Shaqfeh, Dynamic simulation of freely-draining, flexible bead-rod chains: Start-up of extensional and shear flow, J. Nonnewton. Fluid Mech. 76 (1998) 43–78. doi:10.1016/S0377-0257(97)00112-2.

[24] J.S. Hur, E.S.G. Shaqfeh, R.G. Larson, Brownian dynamics simulations of single DNA molecules in shear flow, J. Rheol. (N. Y. N. Y). 44 (2000) 713–742. doi:doi:10.1122/1.551115.

[25] C.M. Schroeder, E.S.G. Shaqfeh, S. Chu, Effect of Hydrodynamic Interactions on DNA Dynamics in Extensional Flow: Simulation and Single Molecule Experiment, Macromolecules. 37 (2004) 9242–9256. doi:10.1021/ma049461l.

[26] C.E. Sing, A. Alexander-Katz, Designed molecular mechanics using self-associating polymers, Soft Matter. 8 (2012) 11871. doi:10.1039/c2sm26276b.

[27] T.T. Perkins, Single Polymer Dynamics in an Elongational Flow, Science (80-.). 276 (1997) 2016–2021. doi:10.1126/science.276.5321.2016.

[28] P. Szymczak, M. Cieplak, Hydrodynamic effects in proteins., J. Phys. Condens. Matter. 23 (2011) 033102. doi:10.1088/0953-8984/23/3/033102.

[29] M. Doi and S. F. Edwards, The theory of polymer dynamics, Oxford University Press Inc., 1986.

[30] Wenli Ouyang, Dissertation: Charateristics of von Willbrand Factor multimer in blood clotting, Lehigh University, 2015.

ETHAN RONG

Phone: (610)751-5241 Email: ethan.rxt.noc@gmail.com
425 Washington Blvd, Jersey City, NJ 07310, USA

EDUCATION

Lehigh University, P.C.Rossin College 2013 to 2015
M.S. in Mechanical Engineering and Mechanics Aug. 2015

- GPA:3.87/4.00
- Thesis: Conformational Changes of vWF multimer Subject to Extensional Flows
- Core Coursework: Numerical Methods in Engineering, Analysis of Algorithm, Math Methods in Engineering I&II, Heat and Mass Transfer, Fluid Mechanics

Tongji University, Department of Mechanical Engineering 2009 to 2013
B.S. in Mechatronics

- GPA: 90.68/100 Major GPA: 93.76/100
- Honors: Academic Excellence Scholarship (twice)

CAREER EXPERIENCE

Inno-Tech Club, Lehigh University, Bethlehem, PA 2014 to 2015

- Set up a club aiming to introduce popular innovative technology in modern times to students via teach-ins and campus activities.
- Got familiar with 3D printing technology and usage of simple 3D printers.

General Electric, China Technology Center, Shanghai, China Summer 2014

- Implemented a tool in C++ which efficiently simulates the solidification process for polymer of specific shape during casting. This tool is used for optimization.

General Motors, Pan AsiaTechnical Auto Center, Shanghai, China Summer 2012

- Designed an integrated triaxial gearbox with detailed parameters which meets the actual production requirement.

First Auto Workshop, Volkswagen Auto, Changchun, China Summer 2011

- Designed standard Connecting-Rods on the basis of QFLBM and used Solidworks to build 3D models.

RESEARCH EXPERIENCE

Conformational Changes of vWF multimer Subject to Extensional Flows 2014 to 2015
Mentor: Prof. Alparslan Oztekin

- Modeled the polymer chain by a sequence of the beads connected by finitely extensible non-linearelastic (FENE) springs and Hookean springs consecutively.
- Used C++ to develop an adaptive time-stepping algorithm to completely eliminate spring-spring crossing.

Taguchi Optimization Spring 2014
Mentor: Prof. John Coulter

- Identified the most important process parameters for fastener products.
- Used Taguchi Parameter Design approach to optimize the parameters to achieve the goal of minimizing the drawing force.

Magnetic Navigation Trace System 2011 to 2013

- Switched the output magnetic signal measured by Gaussmeter to the digital signal by measuring system based on HMC1022.
- Located the markers approximately by using Sequential Algorithm to calculate their non-linear magnetic field and achieved navigation.

TECHNICAL SKILLS

Programming: C, C++, C#, MATLAB, MySQL, Fortran, Latex, PLC
Application: AutoCAD, Solidworks, UG, Microsoft Office, Fluent, Ansys, Multisim, SCM